

Efficient Non-Linear Proper Orthogonal Decomposition (POD)/Galerkin Reduced Order Models with Stable Penalty Enforcement of Boundary Conditions

I. Kalashnikova^{1,2} and M.F. Barone³

¹ Institute for Computational & Mathematical Engineering, Stanford University, Stanford, CA 94305, U.S.A.

² Numerical Analysis and Applications Department, Sandia National Laboratories, P.O. Box 5800, MS 1320, Albuquerque, NM, 87185, U.S.A.

³ Wind Power Technologies Department, Sandia National Laboratories, P.O. Box 5800, MS 1124, Albuquerque, NM, 87185, U.S.A.

SUMMARY

An efficient, stability-preserving model reduction technique for non-linear initial boundary value problems (IBVPs) whose solutions exhibit inherently non-linear dynamics such as metastability and periodic regimes (limit cycles) is developed. The approach is based on the “continuous” Galerkin projection approach, in which the continuous governing equations are projected onto the reduced basis modes in a continuous inner product. The reduced order model (ROM) basis is constructed via a proper orthogonal decomposition (POD). In general, POD basis modes will not satisfy the boundary conditions of the problem. A weak implementation of the boundary conditions in the ROM based on the penalty method is developed. Asymptotic stability of the ROM with penalty-enforced boundary conditions is examined using the energy method, following linearization and localization of the governing equations in the vicinity of a stable steady solution. This analysis, enabled by the fact that a continuous representation of the reduced basis is employed, leads to a model reduction method with an *a priori* stability guarantee. The approach is applied to two non-linear problems: the Allen-Cahn (or “bistable”) equation and a convection-diffusion-reaction (CDR) system representing a tubular reactor. For each of these problems, bounds on the penalty parameters that ensure asymptotic stability of the ROM solutions are derived. The non-linear terms in the equations are handled efficiently using the “best points” interpolation method (BPIM) proposed by Peraire, Nguyen *et al.* in [22, 23]. Numerical experiments reveal that the POD/Galerkin ROMs with stability-preserving penalty boundary treatment for the two problems considered, both without as well as with interpolation, remain stable in a way that is consistent with the solutions to the governing continuous equations, and capture the correct non-linear dynamics exhibited by the exact solutions to these problems. Copyright © 2011 John Wiley & Sons, Ltd.

KEY WORDS: Non-linear reduced order model, Proper Orthogonal Decomposition (POD)/Galerkin projection, “best points” interpolation method (BPIM), Allen-Cahn equation, tubular reactor convection-diffusion-reaction (CDR) system, penalty method.

*Correspondence to: I. Kalashnikova, Numerical Analysis and Applications Department, Sandia National Laboratories, P.O. Box 5800, MS 1320, Albuquerque, NM, 87185, U.S.A. (ikalash@sandia.gov)

1. INTRODUCTION

Many mathematical models in engineering and science applications are described by non-linear partial differential equations (PDEs) whose solutions exhibit inherently non-linear behavior, including static equilibria, transient steady states, periodic or quasi-periodic time-asymptotic regimes and chaotic oscillations. It is well-known that non-linear equations can be very sensitive to initial conditions and parameters appearing in these equations: a slight perturbation of operating conditions can cause the solution of the PDE to change dramatically. The proper characterization of all such solution states becomes particularly important in non-linear control systems applications, in which one may be interested in fine-tuning a system parameter, or input, to yield a particular state or configuration of the governing system. While investigation of stability and sensitivity of non-linear systems can sometimes be carried out analytically using techniques from non-linear analysis [31, 15], numerical bifurcation techniques are required in general. Packages and tools [29] for performing such bifurcation analyses are available; however, these tools are often too computationally expensive for use in a design or analysis setting.

The cost associated with the analysis of non-linear equations has pushed researchers in mathematics and engineering applications to seek modeling and simulation techniques that retain the essential dynamics of a high-fidelity model, but at a much lower computational cost. The basic idea of these “Reduced Order Models” (ROMs) is to use a relatively small number of solutions generated by a high-fidelity simulation to construct a model that is much cheaper computationally, and can be run in real or near-real time. A ROM to be used in predictive, real-time applications is desired to have the following properties:

- (i) Stability: the ROM should be constructed such that it can be ensured *a priori* that the discretization does not introduce into the approximation any non-physical numerical instabilities inconsistent with any physical instabilities exhibited by the exact solutions to the equations being solved; and
- (ii) Efficiency: the non-linear terms in the ROM should be handled in a way that does not invalidate the label *reduced* order model.

Many non-linear ROM techniques are derived from the Proper Orthogonal Decomposition (POD)/Galerkin projection approach [12, 7, 11]. Non-linear POD/Galerkin ROMs have been constructed in a number of applications. An analytical technique based on the POD method and Galerkin projection was presented for the analysis and characterization of inter-area oscillations in stressed power systems in [30]. Dynamical models for bifurcation analysis and control of self-sustained cavity oscillations, also based on the POD/Galerkin approach, were examined by Rowley *et al.* in [20, 19]. In [18], Bizon *et al.* investigated features and limitations of POD models for different snapshot sampling policies for a tubular reactor with recycle. In [21], Agudelo *et al.* presented an application of positive polynomials to the reduction of the number of temperature constraints of a POD-based predictive controller of a similar tubular reactor.

The aim of the present work is to develop an efficient, asymptotically stable model reduction approach based on the Proper Orthogonal Decomposition (POD) and Galerkin projection for non-linear PDEs exhibiting complex non-linear dynamics, such as metastability (stable/unstable fixed points that coalesce or vanish on a long time scale) and periodic, oscillatory regimes (limit cycles). The proposed model reduction technique is based on the “continuous projection” approach: the continuous, governing

PDEs are projected onto the basis modes in a continuous inner product, in common with the perspective of [13, 10, 1, 8, 2, 3]. This approach is fundamentally different from a popular approach, termed the “discrete projection” approach, in which the semi-discrete representation of the governing equations is projected onto a set of discrete modes in a discrete inner product. The primary advantage of the continuous projection approach is that it allows the use of numerical analysis techniques employed by the spectral methods community [26, 25] to determine, *a priori*, the stability and convergence properties of the ROM. Using these techniques, a ROM based on the continuous projection approach can be derived to possess, by construction, a certain stability guarantee. As shown in [1, 8, 2, 3], the stability of the Galerkin projection step of the model reduction procedure can be closely tied to the choice of inner product and the formulation and implementation of the boundary conditions, which are not necessarily inherited from the discretized equation set by a ROM constructed using the continuous Galerkin projection approach. For non-linear equations, the energy method can be applied to the linearized, constant coefficient version of the continuous problem in order to obtain energy inequalities which bound the temporal growth of the solutions to the IBVP in regions where the exact solutions to these equations are asymptotically stable [26, 28]. This analysis allows one to identify *a priori* if a particular choice of inner product is the “correct” inner product – “correct” from the perspective of stability – for a given equation set. A penalty method implementation of the boundary conditions that preserves asymptotic stability of the ROM with boundary treatment – so as to ensure that the boundary condition terms appearing in the ROM do not destabilize the ROM – may be derived as well, also using the energy method. Efficiency of the ROM can be maintained via the “best points” interpolation method (BPIM) of Peraire, Nguyen *et al.* [22, 23].

The remainder of this paper is organized as follows. Section 2 describes the proposed non-linear model reduction procedure. The Proper Orthogonal Decomposition (POD)/Galerkin approach for model reduction is overviewed in Section 2.1. In Section 2.2, the inefficiency of the direct projection of the non-linear terms in building a non-linear ROM for equations possessing strong non-linearities is exhibited. It is shown how efficiency can be recovered by applying the so-called “best points” interpolation method (BPIM) of [22, 23]. The penalty method approach to enforcing boundary conditions is outlined in Section 2.3, and a procedure for studying asymptotic stability of a Galerkin-projected system is described in Section 2.4. In Sections 3 and 4, efficient reduced order models are developed for the non-linear Allen-Cahn (or “bistable”) equation, and a convection-diffusion-reaction (CDR) model of a tubular reactor, respectively. For both problems considered, a penalty implementation of the boundary conditions is formulated and proven to be asymptotically stable for specific ranges of the penalty parameters. Numerical experiments illustrate that the proposed POD reduced order models developed perform well both without and with interpolation of the non-linear terms: the penalty method is effective in enforcing boundary conditions of the Dirichlet, Neumann and Robin kind, and the ROMs are able to correctly capture the “metastability” phenomenon exhibited by the solution to the former equation, and a stable limit cycle exhibited by the solution to the latter system. It is emphasized that the model reduction approach proposed herein and illustrated on these small-scale benchmarks is extendable to more challenging equations and larger scale problems that arise in various industrial and engineering applications, for example non-linear conservation laws in the field of computational fluid dynamics (CFD) (*cf.* [3] for a detailed discussion of an extension of the technique to the full non-linear compressible Navier-Stokes equations). Conclusions are offered in Section 5.

2. CONSTRUCTION AND ANALYSIS OF REDUCED ORDER MODELS FOR NON-LINEAR PDES

2.1. Proper Orthogonal Decomposition (POD)/Galerkin Approach for Model Reduction

This section contains a brief overview of the Proper Orthogonal Decomposition (POD)/Galerkin method for reducing the order of a complex physical system governed by a general set of PDEs. The approach consists of two steps.

The first step is the calculation of a reduced basis using the POD of an ensemble of realizations from a high-fidelity simulation. Discussed in detail in Lumley [6] and Holmes *et al.* [7], POD is a mathematical procedure that, given an ensemble (or snapshot set) of data, denoted by $\{\mathbf{u}^k(\mathbf{x}) : k = 1, \dots, N\}$, constructs a basis for that ensemble that is optimal in the sense that it describes more energy (on average) of the ensemble than any other linear basis of the same dimension M . It is a well-known result [1, 7, 10, 9] that the solution to this optimization problem reduces to the eigenvalue problem $\mathcal{R}\phi = \lambda\phi$ where $\mathcal{R} \equiv \langle \mathbf{u}^k \otimes \mathbf{u}^k \rangle$ is a self-adjoint and positive semi-definite operator. It can be shown [7, 6] that the set of M eigenfunctions, or POD modes, $\{\phi_i : i = 1, 2, \dots, M\}$ corresponding to the M largest eigenvalues of \mathcal{R} is precisely the set of $\{\phi_i\}$ that solves the aforementioned POD optimization. Given this basis, the numerical ROM solution \mathbf{u}_M can be represented as a linear combination of POD modes

$$\mathbf{u}_M(\mathbf{x}, t) = \sum_{j=1}^M a_j(t) \phi_j(\mathbf{x}), \quad (1)$$

where the $a_j(t)$ are the so-called ROM coefficients, to be solved for in the ROM.

The second step in constructing a ROM involves projecting the governing system of PDEs onto the POD basis $\{\phi_i\}$ in some appropriate inner product, denoted generically (for now) by (\cdot, \cdot) . In this step, the full-system dynamics are effectively translated to the implied dynamics of the POD modes. If the governing system of equations for the state variable vector \mathbf{u} has the form

$$\frac{\partial \mathbf{u}}{\partial t} = \mathcal{L}\mathbf{u} + \mathcal{N}_2(\mathbf{u}, \mathbf{u}) + \mathcal{N}_3(\mathbf{u}, \mathbf{u}, \mathbf{u}), \quad (2)$$

where \mathcal{L} is a linear differential operator, and \mathcal{N}_2 and \mathcal{N}_3 are (non-linear) quadratic and cubic operators respectively, then the Galerkin projection of (2) onto the POD mode ϕ_j for $j = 1, 2, \dots, M$ is

$$\left(\phi_j, \frac{\partial \mathbf{u}_M}{\partial t} \right) = \left(\phi_j, \mathcal{L}\mathbf{u}_M \right) + \left(\phi_j, \mathcal{N}_2(\mathbf{u}_M, \mathbf{u}_M) \right) + \left(\phi_j, \mathcal{N}_3(\mathbf{u}_M, \mathbf{u}_M, \mathbf{u}_M) \right). \quad (3)$$

Substituting the POD decomposition of \mathbf{u}_M (1) into (3) and applying the orthonormality property of the basis functions ϕ_i in the inner product (\cdot, \cdot) gives a set of time-dependent ordinary differential equations (ODEs) in the modal amplitudes (also referred to as the ROM coefficients) that accurately describes the flow dynamics of the full system of PDEs for some limited set of flow conditions:

$$\begin{aligned} \frac{da}{dt} \equiv \dot{a}_j &= \sum_{l=1}^M a_l(\phi_j, \mathcal{L}(\phi_l)) + \sum_{l=1}^M \sum_{m=1}^M a_l a_m(\phi_j, \mathcal{N}_2(\phi_l, \phi_m)) \\ &+ \sum_{l=1}^M \sum_{m=1}^M \sum_{n=1}^M a_l a_m a_n(\phi_j, \mathcal{N}_3(\phi_l, \phi_m, \phi_n)), \end{aligned} \quad (4)$$

for $j = 1, 2, \dots, M$.

The approach described herein is based on a Galerkin projection of the *continuous* governing partial differential equations, in common with the perspective of, for example, [10, 13, 1, 8, 2]. This “continuous projection” approach differs from many POD/Galerkin applications, where the semi-discrete representation of the governing equations is projected, and numerical analysis proceeds from the perspective of a dynamical system of ordinary differential equations. The continuous projection approach has the advantage that the ROM solution behavior can be examined using methods that have traditionally been used for numerical analysis of spectral approximations to partial differential equations [26, 25], such as the techniques employed herein in studying stability. Since the stability analysis of the ROM can be done *a priori* at the level of the *continuous* equations, the ROM can be constructed so that its stability is ensured *a priori*. Unlike in the discrete approach, however, in the continuous approach, boundary condition terms present in the discretized equation set are *not* in general inherited by the ROM, and must therefore be implemented separately in the ROM (Section 2.3). It is emphasized that even though a ROM constructed using the discrete projection approach has embedded in it the boundary conditions, many ROMs based on the discrete projection approach are constructed without an *a priori* stability guarantee [14, 4]. These ROMs, though potentially unstable, are nonetheless used in some applications because they can be easier to implement than ROMs constructed using the continuous projection method [1, 4].

For the ROMs developed herein, the standard L^2 inner product is selected for the Galerkin projection step of the model reduction procedure, as the Galerkin projection of the equations considered is asymptotically stable in this inner product (Theorems 3.1.1 and 4.1.1)[†]. In the implementation, the continuous L^2 inner product (\cdot, \cdot) is approximated by a discrete L^2 inner product:

$$(u, v) \equiv \int_{\Omega} uv d\Omega \approx \sum_{k=0}^N u(x_k)v(x_k), \quad (5)$$

where $x_0, \dots, x_N \in \Omega$ are the spatial discretization points.

2.2. “Best Points” Interpolation of Non-Linear Terms in the ROM

Consider the general non-linear IBVP

$$\frac{\partial u}{\partial t} + \mathcal{L}u + \mathcal{N}(u) = f, \quad (6)$$

where \mathcal{L} is a linear operator, \mathcal{N} is a non-linear operator, and f is some source depending on space only (not a function of u). Assume without loss of generality that u is a scalar-valued function. Projecting (6) onto the j^{th} POD (or any reduced basis) mode, denoted by ϕ_j , for $j = 1, \dots, M$, gives rise to a system of ordinary differential equations (ODEs) of the form

$$\dot{\mathbf{a}}_M = \mathbf{F} - \mathbf{L}\mathbf{a}_M - \mathbf{N}(\mathbf{a}_M), \quad (7)$$

where $\mathbf{a}_M^T \equiv (a_1, \dots, a_M)$ and

$$L_{ij} \equiv (\mathcal{L}\phi_j, \phi_i), \quad i, j = 1, \dots, M, \quad (8)$$

[†]Note that for certain systems, e.g., the compressible Euler and Navier-Stokes equations, another inner product may be required to preserve stability of the Galerkin approximation; cf. [1, 8, 2, 3].

$$F_i \equiv (f, \phi_i), \quad i = 1, \dots, M, \quad (9)$$

$$N_i(\mathbf{a}_M) \equiv \left(\mathcal{N} \left(\sum_{k=1}^M a_k \phi_k \right), \phi_i \right), \quad i = 1, \dots, M. \quad (10)$$

The inner products in (10) *cannot* be pre-computed prior to time-integration of the ROM system (7) if \mathcal{N} contains a strong, e.g., a non-polynomial, non-linearity; rather, these inner products would need to be recomputed at each time (or Newton) step of the ROM. This “direct” treatment, or computation, of these inner products can greatly reduce the efficiency of the ROM, and motivates the consideration of some alternative way to handle the non-linearity in (6).

To recover efficiency, the “best points” interpolation of [22, 23], a technique based on a coefficient function approximation for the non-linear terms in (6), is employed. The general procedure is outlined below.

Suppose K snapshots have been taken of the unknown field u , at K different times (the first step of the POD/Galerkin approach for model reduction outlined in Section 2.1):

$$\mathcal{S}^u \equiv \{\xi_k^u(x) = u_h^k(x) : 1 \leq k \leq K\}. \quad (11)$$

Given this set of snapshots of the primal unknown field u , the following set of snapshots of the non-linear function \mathcal{N} appearing in (6) are constructed:

$$\mathcal{S}^{\mathcal{N}} \equiv \{\xi_k^{\mathcal{N}}(x) = \mathcal{N}(u_h^k(x)) : 1 \leq k \leq K\}. \quad (12)$$

The best approximations of the elements in the snapshot set are now defined as:

$$\mathcal{N}_M^*(u_h^k(\cdot)) = \arg \min_{w_M \in \text{span}\{\phi_1^{\mathcal{N}}, \dots, \phi_M^{\mathcal{N}}\}} \|\mathcal{N}(u_h^k(\cdot)) - w_M\|, \quad 1 \leq k \leq K, \quad (13)$$

where the set $\{\phi_m^{\mathcal{N}}\}_{m=1}^M$ is an orthonormal basis for \mathcal{N} , and $\|\cdot\|$ denotes the norm induced by the inner product (\cdot, \cdot) in which the POD basis is constructed (in this work, the standard L^2 inner product (5)). Orthonormality of the $\phi_m^{\mathcal{N}}$ in this inner product implies that

$$\mathcal{N}_M^*(u_h^k(x)) = \sum_{m=1}^M \alpha_m^k \phi_m^{\mathcal{N}}(x), \quad 1 \leq k \leq K, \quad (14)$$

where

$$\alpha_m^k = (\phi_m^{\mathcal{N}}, \mathcal{N}(u_h^k(\cdot))), \quad m = 1, \dots, M, 1 \leq k \leq K. \quad (15)$$

The “best” interpolation points [22, 23], denoted by $\{x_m^{bp}\}_{m=1}^M$, are defined as the solution to the following optimization problem:

$$\min_{x_1^{bp}, \dots, x_M^{bp} \in \Omega} \sum_{k=1}^K \left\| \mathcal{N}_M^*(u_h^k(\cdot)) - \sum_{m=1}^M \beta_m^k(x_1^{bp}, \dots, x_M^{bp}) \phi_m^{\mathcal{N}} \right\|^2, \quad (16)$$

$$\sum_{n=1}^M \phi_n^{\mathcal{N}}(x_m^{bp}) \beta_n^k(x_1^{bp}, \dots, x_M^{bp}) = \mathcal{N}(u_h^k(x_m^{bp})), \quad 1 \leq m \leq M, 1 \leq k \leq K,$$

i.e., the set of points $\{x_m^{bp}\}_{m=1}^M$ is determined to minimize the average error between the interpolants $\mathcal{N}_M^*(\cdot)$ and the best approximations $\mathcal{N}_M^*(\cdot)$. Substituting (14) into (16) and invoking the orthonormality of the $\{\phi_m^{\mathcal{N}}\}_{m=1}^M$, one can show that (16) is equivalent to

$$\min_{x_1^{bp}, \dots, x_M^{bp} \in \Omega} \sum_{k=1}^K \sum_{m=1}^M (\alpha_m^k - \beta_m^k(x_1^{bp}, \dots, x_M^{bp}))^2, \quad (17)$$

$$\sum_{n=1}^M \phi_n^{\mathcal{N}}(x_m^{bp}) \beta_n^k(x_1^{bp}, \dots, x_M^{bp}) = \mathcal{N}(u_h^k(x_m^{bp})), \quad 1 \leq m \leq M, 1 \leq k \leq K.$$

The solution to the least-squares optimization problem (17) can be found using the Levenberg-Marquardt (LM) algorithm, and is typically reached in less than fifteen iterations of the algorithm [23].

Given the “best points” for \mathcal{N} , i.e., the solutions to (17) (or any set of interpolation points), denoted by $\{x_m^{\mathcal{N}}\}_{m=1}^M$, it is straightforward to apply the interpolation procedure outlined in [22, 23] to the non-linear function $\mathcal{N}(u)$ that appears in (6). The first step is to compute snapshots for the non-linear function \mathcal{N} in (6). From these snapshots the interpolation points $\{x_m^{\mathcal{N}}\}_{m=1}^M$ are computed following the approach outlined above (and discussed in detail in Section 2 of [23]). Given $\{x_m^{\mathcal{N}}\}_{m=1}^M$ and $\{\phi_m^{\mathcal{N}}\}_{m=1}^M$, the so-called “cardinal functions”, denoted by $\{\psi_m^{\mathcal{N}}\}_{m=1}^M$, are computed by solving the following linear system[‡]

$$\boldsymbol{\phi}_M^{\mathcal{N}}(x) = \mathbf{A} \boldsymbol{\psi}_M^{\mathcal{N}}(x), \quad (18)$$

where $\boldsymbol{\phi}_M^{\mathcal{N}}(x) = (\phi_1^{\mathcal{N}}(x), \dots, \phi_M^{\mathcal{N}}(x))^T$ and $\boldsymbol{\psi}_M^{\mathcal{N}}(x) = (\psi_1^{\mathcal{N}}(x), \dots, \psi_M^{\mathcal{N}}(x))^T$, and $A_{ij} = \phi_j^{\mathcal{N}}(x_i^{\mathcal{N}})$, with the cardinal functions satisfying $\psi_j^{\mathcal{N}}(x_i) = \delta_{ij}$.

Given the interpolation points $\{x_m^{\mathcal{N}}\}$ and the cardinal functions $\{\psi_m^{\mathcal{N}}\}$, the non-linear function \mathcal{N} is approximated as

$$\mathcal{N}(u) \approx \mathcal{N}_M(u) = \sum_{m=1}^M \mathcal{N}(u(x_m^{\mathcal{N}})) \boldsymbol{\psi}_m^{\mathcal{N}} \in \mathbb{R}, \quad (19)$$

so that

$$\mathcal{N}_M(u) = \sum_{m=1}^M \mathcal{N} \left(\sum_{n=1}^M a_n(t) \phi_n(x_m^{\mathcal{N}}) \right) \boldsymbol{\psi}_m^{\mathcal{N}}, \quad (20)$$

where $\{\phi_m\}_{m=1}^M$ is an orthonormal basis for the primal unknown u , computed from the snapshots (11).

The projection of $\mathcal{N}_M(u)$ (20) onto the l^{th} POD mode for u can be written in matrix/vector form. To do this, note that, for a general function $\mathcal{N}_M(u)$ and for $l = 1, \dots, M$:

$$\begin{aligned} (\phi_l, \mathcal{N}_M(u)) &= (\phi_l, \sum_{m=1}^M \mathcal{N}(\sum_{n=1}^M a_n(t) \phi_n(x_m^{\mathcal{N}})) \boldsymbol{\psi}_m^{\mathcal{N}}) \\ &= \sum_{m=1}^M \left[\int_{\Omega} \phi_l \boldsymbol{\psi}_m^{\mathcal{N}} d\Omega \right] \mathcal{N}(\sum_{n=1}^M a_n(t) \phi_n(x_m^{\mathcal{N}})). \end{aligned} \quad (21)$$

(21) is a matrix/vector product of the form $\mathbf{G}^{\mathcal{N}} \mathcal{N}(\sum_{n=1}^M a_n \phi_n(x_m^{\mathcal{N}}))$ where

$$G_{nm}^{\mathcal{N}} = \int_{\Omega} \phi_n \boldsymbol{\psi}_m^{\mathcal{N}} d\Omega, \quad (22)$$

for $1 \leq m, n \leq M$ (so that $\mathbf{G}^{\mathcal{N}} \in \mathbb{R}^{M \times M}$).

It follows that, with the interpolation procedure described here, the ODE system for the ROM coefficients is not (7) but rather

$$\dot{\mathbf{a}}_M = \mathbf{F} - \mathbf{L} \mathbf{a}_M - \mathbf{G}^{\mathcal{N}} \mathcal{N}(\mathbf{D}^{\mathcal{N}} \mathbf{a}_M), \quad (23)$$

[‡]Note that, for \mathbf{A} to be invertible, the number of interpolation points must be equal to the number of reduced basis modes M . A non-linear least squares optimization problem may be formulated if it is desired to have more interpolation points than modes M , but this latter approach is not considered in the present work.

where \mathbf{F} and \mathbf{L} are defined in (9) and (8) respectively, the entries of the matrix $\mathbf{G}^{\mathcal{N}}$ are given by (22), and

$$\mathbf{D}^{\mathcal{N}} \equiv \begin{pmatrix} \phi_1(x_1^{\mathcal{N}}) & \dots & \phi_M(x_1^{\mathcal{N}}) \\ \vdots & \ddots & \vdots \\ \phi_1(x_M^{\mathcal{N}}) & \dots & \phi_M(x_M^{\mathcal{N}}) \end{pmatrix} \in \mathbb{R}^{M \times M}. \quad (24)$$

To clarify the notation in (23), namely what is meant by a function \mathcal{N} of a vector:

$$\mathcal{N}(\mathbf{D}^{\mathcal{N}} \mathbf{a}_M) \equiv \mathcal{N} \begin{pmatrix} \sum_{m=1}^M a_m(t) \phi_m(x_1^{\mathcal{N}}) \\ \vdots \\ \sum_{m=1}^M a_m(t) \phi_m(x_M^{\mathcal{N}}) \end{pmatrix} \equiv \begin{pmatrix} \mathcal{N}(\sum_{m=1}^M a_m(t) \phi_m(x_1^{\mathcal{N}})) \\ \vdots \\ \mathcal{N}(\sum_{m=1}^M a_m(t) \phi_m(x_M^{\mathcal{N}})) \end{pmatrix} \in \mathbb{R}^M. \quad (25)$$

Once the ROM system (23) is constructed, the ROM is solved by advancing this system forward in time using a standard time-integration scheme (e.g., Euler, Runge-Kutta), or a combination of a time-integration scheme and Newton's method, if the chosen time-integration scheme is implicit.

Essentially, in the BPIM, recomputation of inner products (projection) of the non-linear terms at each time (or Newton) step is replaced by evaluation of the basis functions at the interpolation points. These interpolation points are pre-computed and much fewer in number than N , the number of spatial grid points. Hence, with interpolation, the cost of each step of the online time-integration stage of the model reduction procedure is of $\mathcal{O}(M)$ – compared to $\mathcal{O}(N)$ for the model reduction procedure with interpolation. Since $M \ll N$ in practice, the savings gained in employing the interpolation can be substantial, especially if the governing equation set possesses a strong (non-polynomial) non-linearity $\mathcal{N}(\mathbf{u})$. The computational complexity of the “best points” interpolation algorithm is discussed in detail in [22, 23].

2.3. Penalty-Enforcement of the Boundary Conditions in the ROM

In a POD ROM developed using the continuous projection approach [1, 8, 2], the boundary condition terms present in the discretized equation set from which the POD basis is generated are not inherited automatically by the ROM solution. The usual way to enforce boundary conditions in a ROM constructed using the continuous projection approach is through a weak implementation, that is, by applying them directly into the boundary integrals that arise when the operator \mathcal{L} in (2) is projected onto a mode and integrated by parts [1, 8, 2]. It has been argued, *cf.* [26], that this weak implementation of the boundary conditions does not take into account the fact that the equation should be obeyed arbitrarily close to the boundary. Indeed, numerical experiments demonstrate that a weak implementation in which the boundary data are substituted directly into the boundary integrals does not work well for some POD ROMs, particularly ROMs for equations with Robin boundary conditions: the ROM solution may exhibit significant errors near the boundaries, error that can grow in time and ultimately corrupt the solution in the entire domain.

An alternative to a weak enforcement of the boundary conditions is a penalty enforcement of boundary conditions *cf.* [26, 25, 24]. Formulating a boundary condition using the penalty method amounts to rewriting a boundary value problem as:

$$\begin{cases} \mathbf{u}_t = \mathcal{L}\mathbf{u} + \mathcal{N}\mathbf{u} + \mathbf{f}, & \text{in } \Omega \\ \mathbf{B}\mathbf{u} = \mathbf{h}, & \text{on } \partial\Omega \end{cases} \quad \rightarrow \quad \mathbf{u}_t = \mathcal{L}\mathbf{u} + \mathcal{N}\mathbf{u} + \mathbf{f} - \Gamma(\mathbf{B}\mathbf{u} - \mathbf{h})\delta_{\partial\Omega}, \quad (26)$$

in $\Omega \cup \partial\Omega$. Here, $\mathbf{\Gamma}$ is a diagonal matrix of penalty parameters selected such that stability is preserved, and $\delta_{\partial\Omega}$ is an indicator function marking the boundary $\partial\Omega$:

$$\delta_{\partial\Omega} \equiv \begin{cases} 1, & \text{for } \mathbf{x} \in \partial\Omega \\ 0, & \text{otherwise.} \end{cases} \quad (27)$$

A useful technique for deriving the penalty parameters in $\mathbf{\Gamma}$ such that the Galerkin projection of (26) remains stable is described in [26]. This technique, outlined in Section 2.4, is employed in the analyses performed in Sections 3.1 and 4.1.

2.4. Stability Analysis

For reduced order models for general non-linear problems such as the ones considered herein, the question of numerical stability can be a complicated one. This is because non-linear equations can support (exhibit) stable as well as unstable, sometimes even chaotic, solutions. A ROM for a non-linear equation or system of equations can only be expected to remain numerically stable in regions where the exact solution to the equation(s) is in a stable state.

As illustrated in [28, 26], linear stability of a non-linear system can be examined for a large class of operators if the solutions are smooth. For such problems, it is sufficient to consider the questions of well-posedness and asymptotic stability for the locally linearized, constant coefficient version of the full non-linear problem. The goal, then, in building a non-linear ROM, is to formulate the discrete problem with boundary conditions such that the Galerkin projection of the equations can be asymptotically stable in a way that is consistent with the asymptotic stability of the governing continuous equations. This is done through the selection of an appropriate (stability-preserving) inner product for the given equation set, and the development of a stability-preserving implementation of the prescribed boundary conditions. Numerical stability of the ROM is studied via the energy method. The key steps involved in using the energy method to build a ROM with an *a priori* stability guarantee for any given equation set are summarized below:

Step 1: Select an inner product (\cdot, \cdot) to be used in building the ROM, with a corresponding norm $\|\cdot\|$.

Step 2: Determine the stable steady states supported by the governing non-linear system, e.g., (26).

Step 3: Linearize the spatial terms that appear in the equation set about a constant state \mathbf{u}_0 at which the solution exhibits stable behavior; that is, linearize about a state \mathbf{u}_0 for which $\Re\{\lambda(\mathbf{J}_0)\} < 0$, i.e., the real parts of the eigenvalues of the Jacobian \mathbf{J}_0 , are negative, where

$$\mathbf{J}_0 \equiv \left. \frac{\partial(\mathcal{L} + \mathcal{N})}{\partial \mathbf{u}} \right|_{\mathbf{u}=\mathbf{u}_0}. \quad (28)$$

Step 4: Ensure that the rate of change of the localized (frozen coefficient) and linearized system energy, given by,

$$\frac{1}{2} \frac{d}{dt} \|\mathbf{u}\|^2 = (\mathbf{J}_0 \mathbf{u} + \mathbf{f}, \mathbf{u}), \quad (29)$$

is non-positive (the system energy is non-increasing[§]) – that is, ensure that the Galerkin projection step

[§]Non-increasing system energy is a sufficient condition for stability of the Galerkin scheme.

of the model reduction without boundary treatment is stable in the chosen inner product.

Step 5: If an energy stability bound of the form (29) cannot be shown, return to Step 1 and select an alternative inner product for the model reduction; otherwise, proceed to Step 6.

Step 6: Derive the penalty parameters (the entries of $\mathbf{\Gamma}$) such that the rate of change of the localized (frozen coefficient) and linearized system energy with penalty-enforced boundary treatment, given by,

$$\frac{1}{2} \frac{d}{dt} \|\mathbf{u}\|^2 = (\mathbf{J}_0 \mathbf{u} + \mathbf{f}, \mathbf{u}) - \mathbf{\Gamma} \int_{\partial\Omega} (\mathbf{B}\mathbf{u} - \mathbf{h}) \cdot \mathbf{u} dS, \quad (30)$$

is non-positive (that is, the system energy remains non-increasing following the addition of boundary condition terms).

In the analyses of Sections 3.1 and 4.1, the energy estimate (30) in Step 6 is recast into an algebraic eigenvalue problem, following the procedure of [26].

3. A STABLE POD ROM FOR THE ALLEN-CAHN (OR ‘‘BISTABLE’’) EQUATION

The Allen-Cahn, or ‘‘bistable’’, equation is an example of a semi-linear reaction-diffusion equation. In $(0, T] \times \mathbb{R}^N$, the equation has the form:

$$u_t = \varepsilon \Delta u + f(u), \quad f(u) \equiv u(1 - u^2), \quad (31)$$

where Δ is the usual Laplacian operator, and $\varepsilon > 0$ is a parameter, representing diffusivity. First proposed by S.M. Allen and J.W. Cahn in the 1970s as a model for grain boundary motion in crystalline solids [16], Allen-Cahn equations have become a prototype model for isothermal phase transitions. These equations arise in the study of mechanisms of pattern formation for various phenomena, such as phase transition, morphogenesis, population genetics and chemical reactions.

In the present work, the equation (31) in one spatial dimension (1D) is considered:

$$\begin{cases} u_t = \varepsilon u_{xx} + u(1 - u^2), & x \in (-1, 1), \quad t \in (0, T], \\ u(-1, t) = -1, \quad u(1, t) = 1, & t \in (0, T], \\ u(x, 0) = 0.53x - 0.47 \sin\left(\frac{3}{2}\pi x\right), & x \in (-1, 1). \end{cases} \quad (32)$$

The initial condition and the solution to this IBVP are plotted in Fig. 1. It is straightforward to find the fixed points of (32), namely by setting $f(u^*) = 0$ and solving for u^* . The equation has three uniform fixed points:

$$u^* = \{-1, 0, 1\}. \quad (33)$$

Stability of these states can be studied by computing the Jacobian

$$J(u) \equiv \frac{\partial f}{\partial u} = 1 - 3u^2, \quad (34)$$

and checking its sign when evaluated at each of the steady states. This analysis leads to the conclusion that the middle state is unstable, but the states $u^* = \pm 1$ are attracting. The solutions to the equation (32) exhibit a phenomenon known as ‘‘metastability’’, characterized by relative flatness of the solution close to the stable states, separated by interfaces that may coalesce or vanish on a long time scale [27] (Fig. 1 (b)).

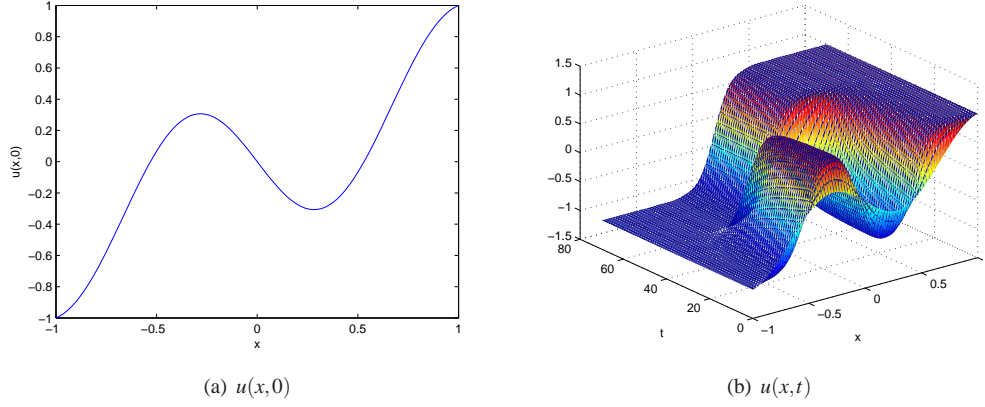


Figure 1. Plots of initial condition and solution to the Allen-Cahn IBVP (32)

3.1. Stability-Preserving Penalty Formulation of Boundary Conditions for the Allen-Cahn Equation

In this section, a stability-preserving penalty enforcement of the boundary conditions for the Allen-Cahn equation (32) is formulated. The first step is to rewrite (32) with a penalty method formulation of the boundary conditions:

$$\begin{cases} u_t = \varepsilon u_{xx} + u(1 - u^2) - \tau_1[u(-1, t) + 1] - \tau_2[u(1, t) - 1], & x \in (-1, 1), \quad t \in (0, T], \\ u(x, 0) = 0.53x - 0.47 \sin\left(\frac{3}{2}\pi x\right), & x \in (-1, 1), \end{cases} \quad (35)$$

for some penalty parameters $\tau_1, \tau_2 \in \mathbb{R}$, to be determined such that the Galerkin projection of (35) in the L^2 inner product is linearly stable (Theorem 3.1.1).

Theorem 3.1.1. *Let $u_0 \in \mathbb{R}$ be a stable steady state for the 1D Allen-Cahn equation (31), so that $J(u_0) \leq 0$ (34). Then the Galerkin projection of the IBVP (35) with a penalty-enforcement of the boundary conditions is asymptotically stable about u_0 if*

$$\tau_1, \tau_2 \geq \underbrace{1 - 3u_0^2}_{J(u_0)} + \frac{1}{4}\varepsilon. \quad (36)$$

Proof. The first step in the analysis is to linearize the function $f(u)$ in (31) about u_0 :

$$u_t \approx \varepsilon u_{xx} + f(u_0) + J(u_0)(u - u_0) = \varepsilon u_{xx} + (1 - 3u_0^2)u + k, \quad (37)$$

where $k \equiv -(1 - 3u_0^2)u_0$ is a constant depending on u_0 . According to the definition of stability (see Definition 2.11 in [5]), it is sufficient to consider the homogeneous version of (37) in studying stability. Therefore, the constant k is neglected from this point forward, and the homogeneous analogs of the

boundary conditions in (35) are considered. Then

$$\begin{aligned}
\frac{1}{2} \frac{d}{dt} \|u\|^2 &= \varepsilon (u_{xx}, u) + (1 - 3u_0^2)(u, u) - \tau_1 u^2(-1, t) - \tau_2 u^2(1, t) \\
&= -\varepsilon \|u_x\|^2 + \varepsilon u(1, t) u_x(1, t) - \varepsilon u(-1, t) u_x(-1, t) + (1 - 3u_0^2) \|u\|^2 - \tau_1 u^2(-1, t) \\
&\quad - \tau_2 u^2(1, t) \\
&\leq -\varepsilon u_x^2(1, t) - \varepsilon u_x^2(-1, t) + \varepsilon u(1, t) u_x(1, t) - \varepsilon u(-1, t) u_x(-1, t) \\
&\quad + (1 - 3u_0^2) u^2(1, t) + (1 - 3u_0^2) u^2(-1, t) - \tau_1 u^2(-1, t) - \tau_2 u^2(1, t) \\
&= (1 - 3u_0^2 - \tau_2) u^2(1, t) + \varepsilon u(1, t) u_x(1, t) - \varepsilon u_x^2(1, t) + (1 - 3u_0^2 - \tau_1) u^2(-1, t) \\
&\quad - \varepsilon u(-1, t) u_x(-1, t) - \varepsilon u_x^2(-1, t) \\
&= \mathbf{u}_R^T \mathbf{H}_R \mathbf{u}_R + \mathbf{u}_L^T \mathbf{H}_L \mathbf{u}_L,
\end{aligned} \tag{38}$$

where

$$\mathbf{H}_R = \frac{1}{2} \begin{pmatrix} 2 - 6u_0^2 - 2\tau_2 & \varepsilon \\ \varepsilon & -2\varepsilon \end{pmatrix}, \quad \mathbf{H}_L = \frac{1}{2} \begin{pmatrix} 2 - 6u_0^2 - 2\tau_1 & -\varepsilon \\ -\varepsilon & -2\varepsilon \end{pmatrix}, \tag{39}$$

and

$$\mathbf{u}_R \equiv \begin{pmatrix} u(1, t) \\ u_x(1, t) \end{pmatrix}, \quad \mathbf{u}_L \equiv \begin{pmatrix} u(-1, t) \\ u_x(-1, t) \end{pmatrix}. \tag{40}$$

In going from step two to step three of (38) the norm identity/inequality

$$-\|u_x\| = -\sum_{j=0}^N u_x^2(x_j) = -u_x^2(-1, t) - u_x^2(1, t) - \sum_{j=1}^{N-1} u_x^2(x_j) \leq -u_x^2(-1, t) - u_x^2(1, t), \tag{41}$$

has been employed (and similarly for $\|u\|$), where $x_j \in (-1, 1)$ are the spatial discretization points employed in the numerical scheme. The fact that, by assumption, $J(u_0) = 1 - 3u_0^2 \leq 0$ (u_0 is a point at which the system is asymptotically stable), has been employed as well.

The eigenvalues of \mathbf{H}_R are:

$$\lambda_{\pm}(\mathbf{H}_R) = \frac{1 - 3u_0^2 - \tau_2 - \varepsilon \pm \sqrt{1 - 6u_0^2 - 2\tau_2 + 2\varepsilon + 9u_0^4 + 6u_0^2\tau_2 - 6u_0^2\varepsilon + \tau_2^2 - 2\tau_2\varepsilon + 2\varepsilon^2}}{2}. \tag{42}$$

Some algebra reveals that these eigenvalues are non-positive if

$$\tau_2 \geq 1 - 3u_0^2 + \frac{1}{4}\varepsilon. \tag{43}$$

By inspection, the matrix \mathbf{H}_L in (39) has the same trace and determinant as the matrix \mathbf{H}_R . It follows that the two matrices have the same eigenvalues. Thus, the condition on τ_1 is the same as the condition on τ_2 , namely (43).

□

To obtain an estimate of what values τ_1 and τ_2 to employ in practice, it is sensible for this example to linearize J about one of the stable fixed points/steady states, namely $u^* = \pm 1$. For these points,

$$J(\pm 1) = -2, \tag{44}$$

so that (36) reduces to the bound

$$\tau_1 \tau_2 \geq -2 + \frac{1}{4}\varepsilon. \tag{45}$$

3.2. Implementation of the Allen-Cahn ROM

The implementation of the Galerkin projection step of the model reduction procedure for the Allen-Cahn IBVP with a penalty enforcement of the boundary conditions (35) is now outlined. Projecting the first line of this IBVP onto the j^{th} POD mode and invoking the orthonormality of the modes gives rise to the following system for the time-dependent ROM coefficient $a_j(t)$ (following an integration by parts on the diffusion term):

$$\begin{aligned} \dot{a}_j &= \sum_{k=1}^M a_k [-\varepsilon(\phi_{k,x}, \phi_{j,x}) + (\phi_k, \phi_j) + \varepsilon[\phi_{k,x}(1)\phi_j(1) - \phi_{k,x}(-1)\phi_j(-1)] \\ &\quad - \tau_1 \phi_k(-1)\phi_j(-1) - \tau_2 \phi_k(1)\phi_j(1)] - \tau_1 \phi_j(-1) + \tau_2 \phi_j(1) + (\mathcal{N}(u_M), \phi_j), \end{aligned} \quad (46)$$

for $j = 1, \dots, M$, where

$$\mathcal{N}(u_M) \equiv -u_M^3, \quad (47)$$

and $u_M \equiv \sum_{k=1}^M a_k(t)\phi_k(x)$.

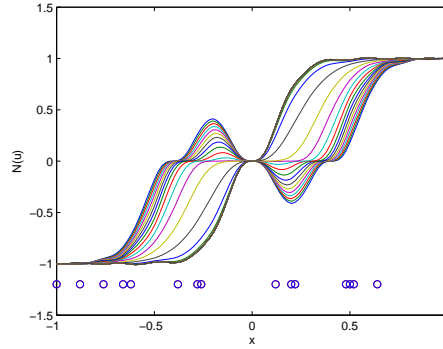


Figure 2. $\mathcal{N}(u)$ (47) (solid lines) and interpolation points (circles) for the Allen-Cahn equation (POD basis, $M = 15$)

Fig. 2 shows the computed “best points” for a POD basis with $M = 15$ (shown in circles), compared with the non-linear function $\mathcal{N}(u)$ (47). Each curve plotted in this figure show $\mathcal{N}(u)$ at a different time t .

3.3. Numerical Results for the Allen-Cahn IBVP

A high-fidelity solution from which snapshots were taken to build the ROM was computed using a Chebyshev collocation spectral method in space and a fourth order Runge-Kutta scheme in time. $N = 101$ spatial discretization points were used, with $\Delta x = 0.02$. The POD basis for the ROM was computed from a total of $K = 40$ snapshots. Twenty of these were snapshots of the solution to (32) with $\varepsilon = 0.02$; the remaining twenty were snapshots of the solution to (32) with $\varepsilon = 0.005$. For each value of the diffusivity, the solution snapshots were saved every $\Delta t_{snap} = 1$ time step until time $T = 20$. Fig. 3 shows the first four POD modes computed for this problem. It is evident that these modes do not satisfy the Dirichlet boundary conditions at $x = \pm 1$.

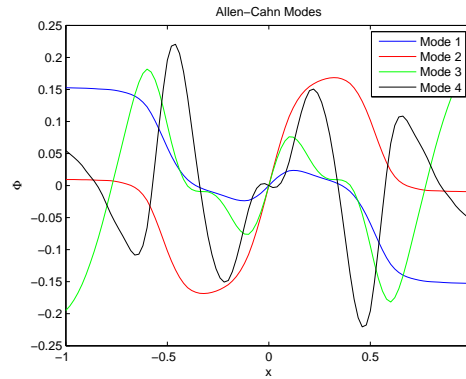


Figure 3. POD modes for the Allen-Cahn equation

In studying the performance of the proposed model reduction procedure, the predictive capability of the ROM is of interest. To this effect, a ROM for (32) with $\varepsilon = 0.001$ is constructed and evaluated. Note that this value of the diffusivity differs from the values of the diffusivity selected in building the reduced basis modes employed in the ROM.

Results (ROM solutions vs. high-fidelity solutions at different times t) for values of $\tau \equiv \tau_1 = \tau_2$ selected within the stable range derived in Theorem 3.1.1 are shown in Fig. 4. For $M \geq 10$, the ROM solution with interpolation looks indistinguishable from the ROM solution without interpolation. Fig. 5 shows time-average errors in the ROM solution relative to the CFD solution at each grid point $x_j \in (-1, 1)$ with τ selected within the stable range (45). The time-average error is defined as

$$\mathcal{E} \equiv \frac{1}{T} \sum_{t_{snap} \leq T} |u_{ROM}(x_j, t_{snap}) - u_{ref}(x_j, t_{snap})|, \quad (48)$$

where the t_{snap} are the times at which the snapshots were taken, u_{ROM} is the ROM solution and u_{ref} is a high-fidelity reference solution, employed in the error analysis in place of the exact solution, as the latter is unavailable analytically for this problem. The accuracy of the ROM with interpolation is comparable to the accuracy of the ROM with a direct treatment of the non-linear term (47) at most of the grid points. Fig. 5 (b) shows a close up of the errors near the left boundary, $x = -1$. Although the ROM remains stable for $\tau = 0$ (a value within the stability region (45)), it is evident from this plot that the Dirichlet boundary condition at this boundary is being enforced with some error. This situation improves by selecting a larger τ . The time-average error (48) at the point $x = -1$ is plotted as a function of τ , for $\tau \in [0, 100]$ in Fig. 6. The reader may observe by examining this figure the convergence of the solution at the left boundary with increasing penalty parameter.

As expected, the ROM goes unstable if τ is selected outside the stability range derived in Theorem 3.1.1 (Fig. 7). In this ROM, the non-linear term is handled directly, so the instability cannot be attributed to a poor set of interpolation points.

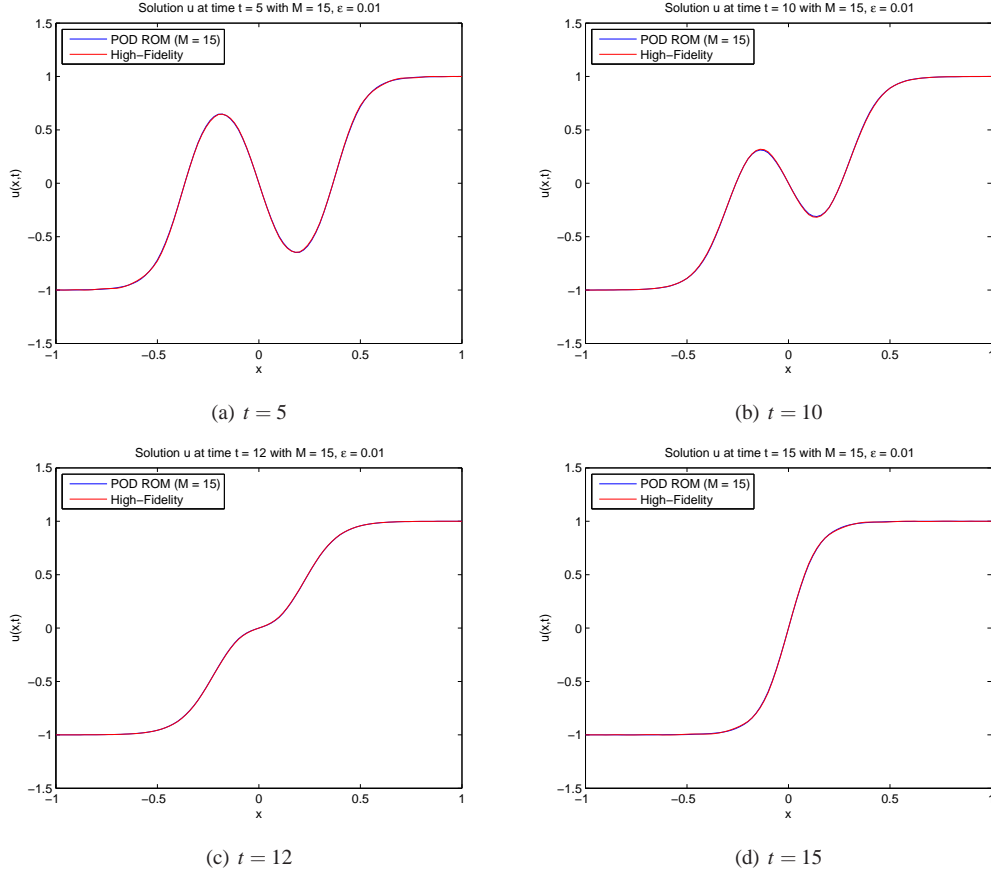


Figure 4. POD ROM solutions to the Allen-Cahn equation with $M = 15$ modes, $\varepsilon = 0.01$, $\tau_1 = \tau_2 = 100$ (with interpolation)

4. A STABLE POD ROM FOR A TUBULAR REACTOR WITH OSCILLATORY REGIMES

In this section, a reduced order model for a non-linear system exhibiting more complex non-linear dynamics than the Allen-Cahn equation considered in Section 3, namely oscillatory regimes, is developed. The mathematical model is that of a one-dimensional (1D) non-adiabatic tubular reactor, represented by a non-linear convection-diffusion-reaction (CDR) system with a single $A \rightarrow B$ reaction [17]. In dimensionless form, the governing equations, describing the conservation of reactant A and energy for the non-adiabatic tubular reactor with mixing are[†]:

$$\begin{aligned} \frac{\partial y}{\partial t} &= \frac{1}{Pe_M} \frac{\partial^2 y}{\partial x^2} - \frac{\partial y}{\partial x} - D(y+1)e^{\frac{\gamma\theta}{\theta+1}}, & x \in (0, 1), \quad t \in [0, T), \\ \frac{\partial \theta}{\partial t} &= \frac{1}{Pe_H} \frac{\partial^2 \theta}{\partial x^2} - \frac{\partial \theta}{\partial x} - \beta(\theta+1-\theta_0) + BD(y+1)e^{\frac{\gamma\theta}{\theta+1}}, & x \in (0, 1), \quad t \in [0, T), \end{aligned} \quad (49)$$

[†]Note that the equations (49)–(52) are exactly the equations considered in [17], but with the transformation $y \leftarrow y+1$, $\theta \leftarrow \theta+1$.

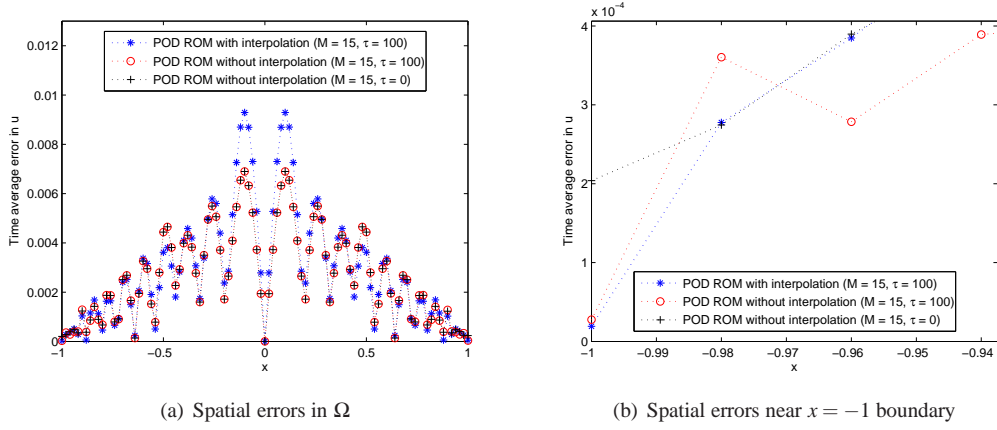


Figure 5. Time-average errors for the ROM solutions to the Allen-Cahn equation with $M = 15$ modes, $\varepsilon = 0.01$, different $\tau \equiv \tau_1 = \tau_2$

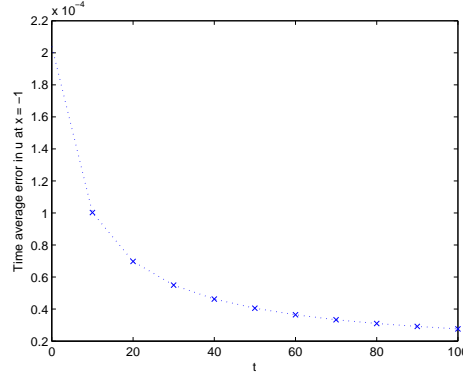


Figure 6. Time-average errors for the ROM solutions to the Allen-Cahn equation with $M = 15$ modes, $\varepsilon = 0.01$ at the left boundary $x = -1$ as a function of $\tau \equiv \tau_1 = \tau_2$

for $\theta_0 \in \mathbb{R}$, $Pe_M, Pe_H > 0$, subject to boundary conditions

$$\begin{cases} \frac{\partial y}{\partial x}|_{x=0} = Pe_M y|_{x=0}, & t \in (0, T], \\ \frac{\partial \theta}{\partial x}|_{x=0} = Pe_H \theta|_{x=0}, & t \in (0, T], \end{cases} \quad (50)$$

$$\begin{cases} \frac{\partial y}{\partial x}|_{x=1} = 0, & t \in (0, T], \\ \frac{\partial \theta}{\partial t}|_{x=1} = 0, & t \in (0, T], \end{cases} \quad (51)$$

and initial conditions

$$y|_{t=0} = y_{in}, \quad \theta|_{t=0} = \theta_{in}, \quad x \in (0, 1). \quad (52)$$

Here, y is the dimensionless concentration, θ is the dimensionless temperature, x is the dimensionless axial distance, t is the dimensionless time, β is the dimensionless heat transfer coefficient, γ is the

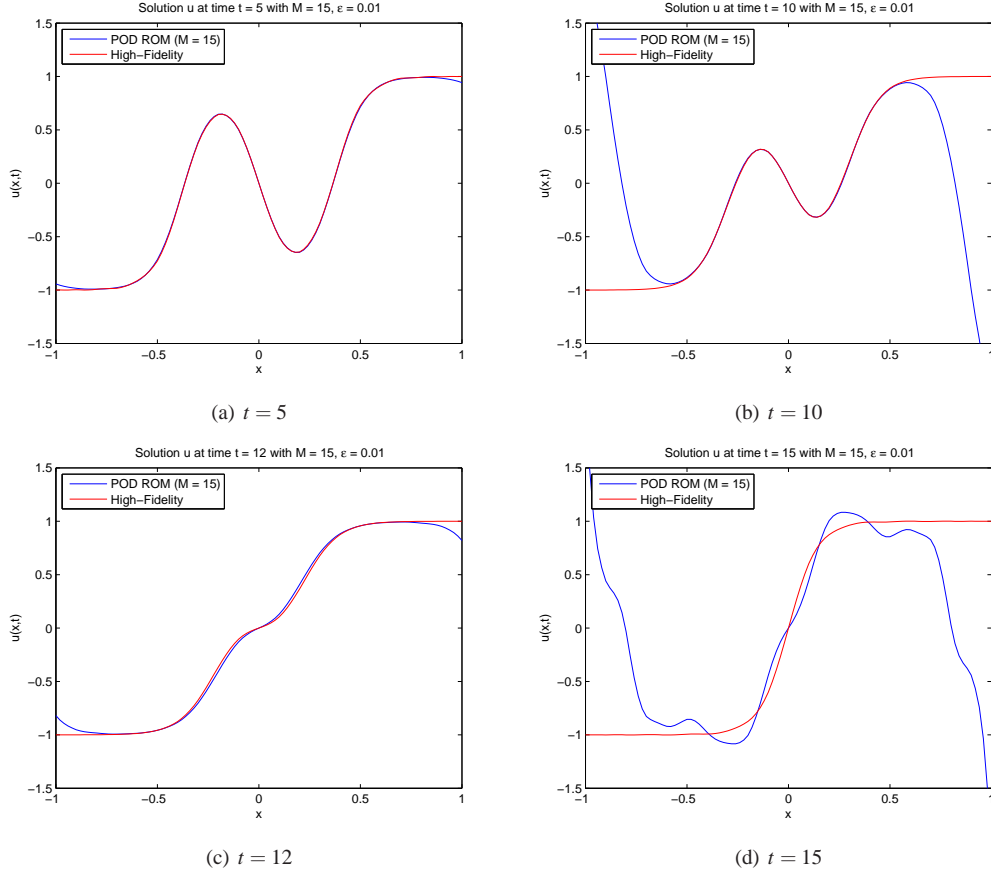


Figure 7. POD ROM solutions to the Allen-Cahn equation with $M = 15$ modes, $\varepsilon = 0.01$, $\tau_1 = \tau_2 = -10$ (no interpolation)

dimensionless activation energy, D is the Damköhler number, B is the dimensionless heat of reaction, and Pe_M and Pe_H are the Péclet numbers for mass and heat transfer respectively. The boundary conditions enforced are of a mixed form: Neumann at the right boundary $x = 1$ (51) and Robin at the left boundary $x = 0$ (50).

It is convenient to write (49)–(52) in vector form, as follows:

$$\begin{cases} \frac{\partial \mathbf{u}}{\partial t} = \mathbf{P} \frac{\partial^2 \mathbf{u}}{\partial x^2} - \frac{\partial \mathbf{u}}{\partial x} - \mathbf{B}(\mathbf{u} + \mathbf{e}_2 - \mathbf{u}_0) - \mathbf{C}\mathcal{N}(\mathbf{u}), & x \in (0, 1), \quad t \in (0, T], \\ \mathbf{P} \frac{\partial \mathbf{u}}{\partial x} \Big|_{x=0} = \mathbf{u} \Big|_{x=0}, & t \in (0, T] \\ \frac{\partial \mathbf{u}}{\partial x} \Big|_{x=1} = \mathbf{0}, & t \in (0, T], \\ \mathbf{u}(x, 0) = \mathbf{u}_{in}, & x \in (0, 1), \end{cases} \quad (53)$$

where, for $y_0 \in \mathbb{R}$,

$$\mathbf{u} \equiv \begin{pmatrix} y \\ \theta \end{pmatrix}, \quad \mathbf{u}_0 \equiv \begin{pmatrix} y_0 \\ \theta_0 \end{pmatrix}, \quad \mathbf{u}_{in} \equiv \begin{pmatrix} y_{in} \\ \theta_{in} \end{pmatrix}, \quad (54)$$

$$\mathbf{P} \equiv \begin{pmatrix} Pe_M^{-1} & 0 \\ 0 & Pe_H^{-1} \end{pmatrix}, \quad \mathbf{B} \equiv \begin{pmatrix} 0 & 0 \\ 0 & \beta \end{pmatrix}, \quad \mathbf{C} \equiv \begin{pmatrix} D \\ -BD \end{pmatrix}, \quad \mathbf{e}_2 \equiv \begin{pmatrix} 0 \\ 1 \end{pmatrix}, \quad (55)$$

and

$$\mathcal{N}(\mathbf{u}) \equiv (y+1)e^{\frac{\gamma\theta}{\theta+1}} \in \mathbb{R}. \quad (56)$$

The fixed points of (49) are the zeros of the non-linear function (56). By inspection, it is straightforward to see that $(y^*, \theta^*) = (-1, k)$, for any $k \in \mathbb{R}$ is a family of fixed points.

Let

$$\mathbf{f}(y, \theta) \equiv \begin{pmatrix} -D(y+1)e^{\frac{\gamma\theta}{\theta+1}} \\ -\beta\theta + BD(y+1)e^{\frac{\gamma\theta}{\theta+1}} \end{pmatrix} = -\mathbf{B}\mathbf{u} - \mathbf{C}\mathcal{N}(\mathbf{u}). \quad (57)$$

The Jacobian of (57) is given by

$$\mathbf{J}(\mathbf{u}) \equiv \frac{\partial \mathbf{f}}{\partial \mathbf{u}} = \begin{pmatrix} -D & -D\gamma h(\mathbf{u}) \\ BD & -\beta + BD\gamma h(\mathbf{u}) \end{pmatrix} g(\theta), \quad (58)$$

where

$$h(\mathbf{u}) \equiv \frac{y+1}{(\theta+1)^2}, \quad g(\theta) \equiv e^{\frac{\gamma\theta}{\theta+1}}. \quad (59)$$

The eigenvalues of $\mathbf{J}(\mathbf{u})$ are:

$$\lambda_{1,2} = \frac{g(\theta)}{2} \left(BD\gamma h(\mathbf{u}) - D - \beta \pm \sqrt{D^2 - 2D\beta - 2D^2\gamma h(\mathbf{u})B + \beta^2 - 2\beta BD\gamma h(\mathbf{u}) + B^2 D^2 \gamma^2 h^2(\mathbf{u})} \right). \quad (60)$$

It is apparent (since $\mathbf{J}(-1, k)$ is lower triangular) that $\lambda\{\mathbf{J}(-1, k)\} = -De^{\frac{\gamma k}{k+1}}, -\beta e^{\frac{\gamma k}{k+1}}$, both of which are necessarily negative, meaning $(y^*, \theta^*) = (-1, k)$, for $k \in \mathbb{R}$ defines a region of stable solutions.

As it turns out, the dynamics of the non-linear problem (49) are more complex than those of the Allen-Cahn equation considered above. These behaviors are studied using numerical bifurcation techniques [17], which reveal periodic solutions possessing Hopf bifurcations, and multiplicity patterns exhibiting from one to seven steady states. The existence of stable oscillatory solutions as a function of the Damköhler number D when $Pe_M = Pe_H = 5$, $B = 0.50$, $\gamma = 25$, $\beta = 2.5$ and $\theta_0 = 1$ can be shown. In particular, there is a stable orbit that bifurcates into a limit cycle at the lower Hopf point, $D = 0.165$ (Fig. 13).

4.1. Stability-Preserving Penalty Formulation of Boundary Conditions for the Tubular Reactor Problem

The penalty formulation of (49) with boundary conditions (50) and (51) is

$$\frac{\partial \mathbf{u}}{\partial t} = \mathbf{P} \frac{\partial^2 \mathbf{u}}{\partial x^2} - \frac{\partial \mathbf{u}}{\partial x} - \mathbf{B}(\mathbf{u} + \mathbf{e}_2 - \mathbf{u}_0) - \mathbf{C}\mathcal{N}(\mathbf{u}) - \tau_1 \left(\mathbf{u}|_{x=0} - \mathbf{P} \frac{\partial \mathbf{u}}{\partial x} \Big|_{x=0} \right) - \tau_2 \frac{\partial \mathbf{u}}{\partial x} \Big|_{x=1}, \quad (61)$$

for some penalty parameters $\tau_1, \tau_2 \in \mathbb{R}$ (to be determined).

As with the Allen-Cahn equation, linear stability of the penalty-formulation of the boundary conditions for the CDR tubular reactor problem (61) is studied following a linearization of the non-linear function that appears in this system. Suppose that \mathbf{f} (57) has been linearized about some stable state \mathbf{u}_0 :

$$\mathbf{f}(\mathbf{u}) \approx \mathbf{f}(\mathbf{u}_0) + \mathbf{J}(\mathbf{u}_0)(\mathbf{u} - \mathbf{u}_0) = \mathbf{J}(\mathbf{u}_0)\mathbf{u} + \mathbf{c}, \quad (62)$$

for some constant vector $\mathbf{c} \in \mathbb{R}^2$ depending on \mathbf{u}_0 . Introducing the shorthand $\mathbf{J}_0 \equiv \mathbf{J}(\mathbf{u}_0)$, it follows that the linearized variant of (61), written in vector form is

$$\mathbf{u}_t = \mathbf{P}\mathbf{u}_{xx} - \mathbf{u}_x + \mathbf{J}_0\mathbf{u} + \mathbf{c} - \tau_1 [\mathbf{u}(0,t) - \mathbf{P}\mathbf{u}_x(0,t)] - \tau_2\mathbf{u}_x(1,t), \quad (63)$$

where \mathbf{P} is given by (55).

An energy stability analysis applied to (63) gives bounds on the penalty parameters τ_1 and τ_2 such that the Galerkin projection of these equations in the L^2 inner product is asymptotically stable about a stable state \mathbf{u}_0 (Theorem 4.1.1).

Theorem 4.1.1. *Let $\mathbf{u}_0^T \equiv (y_0, \theta_0) \in \mathbb{R}^2$ be a stable point for the convection-diffusion-reaction tubular reactor system (49), so that $\mathcal{R}\{\lambda(\mathbf{J}(\mathbf{u}_0))\} \leq 0$. Then the Galerkin projection of the IBVP with a penalty-enforcement of the boundary conditions is asymptotically stable about \mathbf{u}_0 if*

$$\max_{i=1,2} \left\{ 0, 2Pe + 1 - \sqrt{4Pe^2 + 2Pe - 4Pe\lambda_0^i} \right\} \leq \tau_1 \leq \min_{i=1,2} \left\{ 2Pe + 1 + \sqrt{4Pe^2 + 2Pe - 4Pe\lambda_0^i} \right\}, \quad (64)$$

$$\max_{i=1,2} \left\{ \frac{1 - \sqrt{2Pe - 4Pe\lambda_0^i}}{Pe} \right\} \leq \tau_2 \leq \min_{i=1,2} \left\{ \frac{1 + \sqrt{2Pe - 4Pe\lambda_0^i}}{Pe} \right\}, \quad (65)$$

where λ_0^i , $i = 1, 2$ are the eigenvalues of $\mathbf{J}_0 \equiv \mathbf{J}(\mathbf{u}_0)$ (58), and $Pe = \min\{Pe_M, Pe_H\}^\parallel$.

Proof. Let $Pe \equiv \min\{Pe_M, Pe_H\}$ and assume $Pe_M = Pe_H > 0$, $\tau_1 \geq 0$. Then

$$\mathbf{u}_t \leq Pe^{-1}\mathbf{u}_{xx} - \mathbf{u}_x + \mathbf{J}_0\mathbf{u} + \mathbf{c} - \tau_1 [\mathbf{u}(0,t) - Pe^{-1}\mathbf{u}_x(0,t)] - \tau_2\mathbf{u}_x(1,t), \quad (66)$$

The two equations in (66) are coupled by the Jacobian matrix \mathbf{J}_0 . These equations can be decoupled by diagonalizing \mathbf{J}_0 :

$$\mathbf{J}_0 = \mathbf{S}_0\mathbf{\Lambda}_0\mathbf{S}_0^{-1}, \quad (67)$$

where

$$\mathbf{\Lambda}_0 \equiv \begin{pmatrix} \lambda_0^1 & 0 \\ 0 & \lambda_0^2 \end{pmatrix}, \quad (68)$$

is a diagonal matrix containing the eigenvalues of \mathbf{J}_0 , and \mathbf{S}_0 is a matrix with columns spanned by the normalized eigenvectors of \mathbf{J}_0 . Let

$$\mathbf{v} \equiv \mathbf{S}_0^{-1}\mathbf{u}. \quad (69)$$

In these variables, (66) becomes

$$\mathbf{v}_t \leq Pe^{-1}\mathbf{v}_{xx} - \mathbf{v}_x + \mathbf{\Lambda}_0\mathbf{v} + \mathbf{S}_0^{-1}\mathbf{c} - \tau_1 [\mathbf{v}(0,t) - Pe^{-1}\mathbf{v}_x(0,t)] - \tau_2\mathbf{v}_x(1,t), \quad (70)$$

or, equivalently,

$$\begin{cases} v_{1,t} & \leq Pe^{-1}v_{1,xx} - v_{1,x} + \lambda_0^1 v_1 - \tau_1 [v_1(0,t) - Pe^{-1}v_{1,x}(0,t)] - \tau_2 v_{1,x}(1,t), \\ v_{2,t} & \leq Pe^{-1}v_{2,xx} - v_{2,x} + \lambda_0^2 v_2 - \tau_1 [v_2(0,t) - Pe^{-1}v_{2,x}(0,t)] - \tau_2 v_{2,x}(1,t), \end{cases} \quad (71)$$

^{||}Note that the range for τ_2 (65) is necessarily defined, as $\lambda_0^i < 0$ and $Pe > 0$.

where $\mathbf{v}^T \equiv (v_1, v_2)$.

Each of the components in (71) is considered one at a time. Setting $\mathbf{c} = \mathbf{0}$ and using the identity $(v_{1,x}, v) \equiv \frac{1}{2} \int_{\Omega} (v^2)_x dx$ as well as (41):

$$\begin{aligned}
\frac{1}{2} \frac{d}{dt} \|v_1\|^2 &\leq Pe^{-1}(v_{1,xx}, v_1) - (v_{1,x}, v_1) + \lambda_0^1(v_1, v_1) - \tau_1(v_1(0, t) - Pe^{-1}v_{1,x}(0, t))v_1(0, t) \\
&\quad - \tau_2 v_{1,x}(1, t)v_1(1, t) \\
&= -Pe^{-1}\|v_{1,x}\|^2 + Pe^{-1}v_{1,x}(1, t)v(1, t) - Pe^{-1}v_{1,x}(0, t)v(0, t) - \frac{1}{2}v_1^2(1, t) \\
&\quad + \frac{1}{2}v_1^2(0, t) + \lambda_0^1\|v_1\|^2 - \tau_1 v_1^2(0, t) + \tau_1 Pe^{-1}v_{1,x}(0, t)v_1(0, t) - \tau_2 v_{1,x}(1, t)v_1(1, t) \\
&\leq -Pe^{-1}v_{1,x}^2(0, t) - Pe^{-1}v_{1,x}^2(1, t) + Pe^{-1}v_{1,x}(1, t)v(1, t) - Pe^{-1}v_{1,x}(0, t)v_1(0, t) \\
&\quad - \frac{1}{2}v_1^2(1, t) + \frac{1}{2}v_1^2(0, t) + \lambda_0^1 v_1^2(0, t) + \lambda_0^1 v_1^2(1, t) - \tau_1 v_1^2(0, t) + \tau_1 Pe^{-1}v_{1,x}(0, t)v_1(0, t) \\
&\quad - \tau_2 v_{1,x}(1, t)v_1(1, t) \\
&= \left(\frac{1}{2} + \lambda_0^1 - \tau_1\right) v_1^2(0, t) + (\tau_1 Pe^{-1} - Pe^{-1}) v_{1,x}(0, t)v_1(0, t) - Pe^{-1}v_{1,x}^2(0, t) \\
&\quad + \left(-\frac{1}{2} + \lambda_0^1\right) v_1^2(1, t) + (Pe^{-1} - \tau_2) v_{1,x}(1, t)v_1(1, t) - Pe^{-1}v_{1,x}^2(1, t) \\
&= \mathbf{v}_{1L}^T \mathbf{H}_{1L} \mathbf{v}_{1L} + \mathbf{v}_{1R}^T \mathbf{H}_{1R} \mathbf{v}_{1R},
\end{aligned} \tag{72}$$

where

$$\mathbf{H}_{1L} \equiv \frac{1}{2Pe} \begin{pmatrix} Pe(1 + 2\lambda_0^1 - 2\tau_1) & \tau_1 - 1 \\ \tau_1 - 1 & -2 \end{pmatrix}, \quad \mathbf{H}_{1R} \equiv \frac{1}{2Pe} \begin{pmatrix} Pe(-1 + 2\lambda_0^1) & 1 - Pe\tau_2 \\ 1 - Pe\tau_2 & -2 \end{pmatrix}, \tag{73}$$

and

$$\mathbf{v}_{1L} \equiv \begin{pmatrix} v_1(0, t) \\ v_{1,x}(0, t) \end{pmatrix}, \quad \mathbf{v}_{1R} \equiv \begin{pmatrix} v_1(1, t) \\ v_{1,x}(1, t) \end{pmatrix}. \tag{74}$$

The eigenvalues of \mathbf{H}_{1L} are:

$$\lambda\{\mathbf{H}_{1L}\} = \frac{1}{2}\lambda_0^1 + \frac{1}{4} - \frac{1}{2}\tau_1 - \frac{1}{2Pe} \pm \frac{1}{4Pe} \sqrt{\Delta_{1L}}, \tag{75}$$

where

$$\begin{aligned}
\Delta_{1L} &\equiv 4Pe^2(\lambda_0^1)^2 + 4Pe^2\lambda_0^1 - 8Pe^2\lambda_0^1\tau_1 + 8Pe\lambda_0^1 + Pe^2 - 4Pe^2\tau_1 + 4Pe + 4Pe^2\tau_1^2 \\
&\quad - 8Pe\tau_1 + 8 - 8\tau_1 + 4\tau_1^2.
\end{aligned} \tag{76}$$

Some algebra reveals that these eigenvalues are non-positive if

$$2Pe + 1 - \sqrt{4Pe^2 + 2Pe - 4Pe\lambda_0^1} \leq \tau_1 \leq 2Pe + 1 + \sqrt{4Pe^2 + 2Pe - 4Pe\lambda_0^1}. \tag{77}$$

Similarly, the eigenvalues of \mathbf{H}_{1R} are:

$$\lambda\{\mathbf{H}_{1R}\} = \frac{1}{2}\lambda_0^1 - \frac{1}{4} - \frac{1}{2Pe} \pm \frac{1}{4Pe} \sqrt{\Delta_{1R}}, \tag{78}$$

where

$$\Delta_{1R} \equiv Pe^2 - 4\lambda_0^1 Pe^2 - 4Pe + 4Pe^2(\lambda_0^1)^2 + 8Pe\lambda_0^1 + 8 - 8\tau_2 Pe + 4\tau_2^2 Pe^2. \tag{79}$$

It is straightforward to show that (78) is non-positive for

$$\frac{1 - \sqrt{2Pe - 4Pe\lambda_0^1}}{Pe} \leq \tau_2 \leq \frac{1 + \sqrt{2Pe - 4Pe\lambda_0^1}}{Pe}. \tag{80}$$

The equation for v_2 is the same as the equation for v_1 , but with λ_0^1 replaced by λ_0^2 . The stability analysis, therefore, is the same as well. It follows that the bounds (64) and (65) on τ_1 and τ_2 respectively are sufficient conditions for ensuring asymptotic stability of the Galerkin projection of the tubular reactor equations with a penalty-enforcement of the boundary conditions (61).

□

4.2. Implementation of the Tubular Reactor CDR ROM

A scalar POD basis is built for each of the unknowns, y and θ :

$$y(x, t) \approx y_M(x, t) = \sum_{m=1}^M a_m^y(t) \phi_m^y(x), \quad (81)$$

$$\theta(x, t) \approx \theta_M(x, t) = \sum_{m=1}^M a_m^\theta(t) \phi_m^\theta(x). \quad (82)$$

The POD modes ϕ_m^y are constructed from snapshots of the concentration y only; the POD modes ϕ_m^θ are constructed from snapshots of the temperature θ only. Note that one could, as an alternative, construct a vector basis $\boldsymbol{\phi} \in \mathbb{R}^2$ from snapshots of the vector $(y, \theta)^T \in \mathbb{R}^2$. Numerical experiments reveal that employing scalar bases for each of the variables (81) and (82) yields a slightly more accurate ROM for a fixed number of dofs for this problem.

The ROM is constructed by projecting the y equation in (63) onto ϕ_j^y and the θ equation in (63) onto ϕ_j^θ in the L^2 inner product, for $j = 1, \dots, M$. Projecting the concentration equation onto the j^{th} POD mode, the following expression is obtained, after performing an integration by parts on the diffusion term and substituting the modal representation of the concentration:

$$\begin{aligned} \dot{a}_j^y &= -\sum_{k=1}^M a_k^y \left\{ \frac{1}{Pe_M} \left(\frac{\partial \phi_k^y}{\partial x}, \frac{\partial \phi_j^y}{\partial x} \right) + \left(\frac{\partial \phi_k^y}{\partial x}, \phi_j^y \right) + \frac{1}{Pe_M} \left[\frac{\partial \phi_k^y}{\partial x} \Big|_{x=1} \phi_j^y(1) - \frac{\partial \phi_k^y}{\partial x} \Big|_{x=0} \phi_j^y(0) \right] \right. \\ &\quad \left. - \tau_1 \left(\phi_k^y(0) - \frac{1}{Pe_M} \frac{\partial \phi_k^y}{\partial x} \Big|_{x=0} \right) \phi_j^y(0) - \tau_2 \frac{\partial \phi_k^y}{\partial x} \Big|_{x=1} \phi_j^y(1) \right\} - D \left(\mathcal{N}(\mathbf{u}_M), \phi_j^y \right), \end{aligned} \quad (83)$$

where $\mathcal{N}(\mathbf{u}_M)$ is defined in (56). Similarly, for the temperature equation:

$$\begin{aligned} \dot{a}_j^\theta &= -\sum_{k=1}^M a_k^\theta \left\{ \frac{1}{Pe_H} \left(\frac{\partial \phi_k^\theta}{\partial x}, \frac{\partial \phi_j^\theta}{\partial x} \right) + \left(\frac{\partial \phi_k^\theta}{\partial x}, \phi_j^\theta \right) + \beta \left(\phi_k^\theta, \phi_j^\theta \right) \right. \\ &\quad \left. + \frac{1}{Pe_H} \left[\frac{\partial \phi_k^\theta}{\partial x} \Big|_{x=1} \phi_j^\theta(1) - \frac{\partial \phi_k^\theta}{\partial x} \Big|_{x=0} \phi_j^\theta(0) \right] - \tau_1 \left(\phi_k^\theta(0) - \frac{1}{Pe_H} \frac{\partial \phi_k^\theta}{\partial x} \Big|_{x=0} \right) \phi_j^\theta(0) \right. \\ &\quad \left. - \tau_2 \frac{\partial \phi_k^\theta}{\partial x} \Big|_{x=1} \phi_j^\theta(1) \right\} + \beta(1 - \theta_0, \phi_j^\theta) + BD \left(\mathcal{N}(\mathbf{u}_M), \phi_j^\theta \right). \end{aligned} \quad (84)$$

In total, there are $2M$ unknowns: $\{a_j^y, a_j^\theta : j = 1, \dots, M\}$. To estimate a desirable range of τ_1 and τ_2 , a stable point (y_0, θ_0) in the vicinity of the limit cycle is selected and the result of Theorem 4.1.1 is applied (Section 4.3).

Both systems (83) and (84) contain the following non-linearity:

$$\left(\mathcal{N}(\mathbf{u}_M), \phi_j \right) = \left(\left(\sum_{m=1}^M a_m^y(t) \phi_m^y(x) + 1 \right) \exp \left\{ \frac{\gamma \sum_{m=1}^M a_m^\theta(t) \phi_m^\theta(x)}{\sum_{m=1}^M a_m^\theta(t) \phi_m^\theta(x) + 1} \right\}, \phi_j \right), \quad (85)$$

which clearly cannot be precomputed prior to time-integration of the ROM, and hence must be recomputed at each time step of the time-integration scheme employed with the “direct” treatment of the non-linearity (85). This approach is extremely costly. However, the interpolation outlined in Section 2.2 can be employed to recover efficiency of the ROM**. The interpolation points computed for the scalar function $\mathcal{N}(\mathbf{u})$ (56) with $M = 5$ are plotted in Fig. 8 along with this non-linear function, shown for different times t .

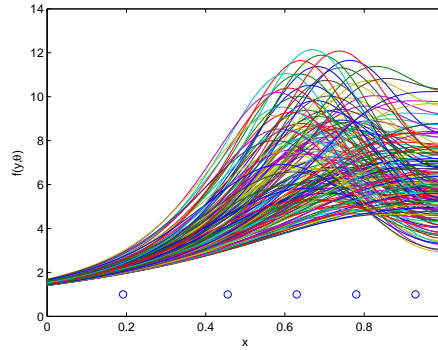


Figure 8. $\mathcal{N}(\mathbf{u})$ (56) (solid lines) and interpolation points (circles) for the tubular reactor CDR system (POD basis, $M = 5$)

4.3. Numerical Results for the Tubular Reactor CDR System

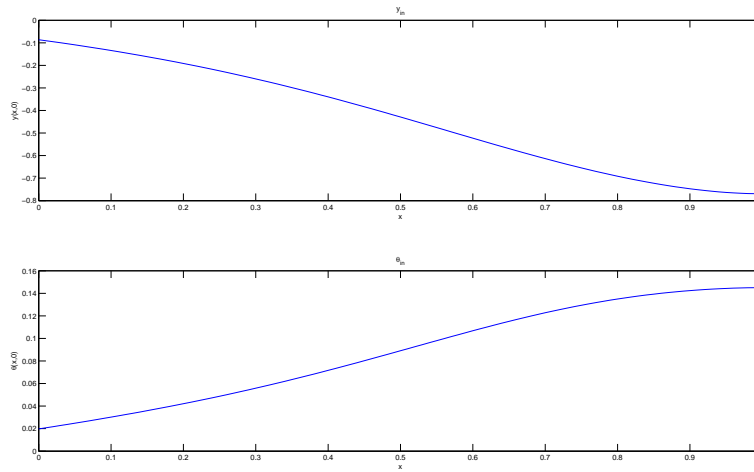
The high-fidelity solution to the tubular reactor CDR system was obtained using a Fourier spectral Galerkin method in space, and a fourth order Runge-Kutta time-integration scheme. The domain $\Omega = (0, 1)$ was discretized by $N = 101$ spatial discretization points, so that $\Delta x = 0.01$. The initial conditions y_{in} and θ_{in} , plotted in Fig. 9, were calculated using an implicit relation scheme for the steady state solution. The values of the parameters for the solution from which the snapshots were taken are summarized in Table I. For a value of the Damkhöler number in the range $0.165 \leq D \leq 0.17$, the solution is known to exhibit a stable limit cycle (Fig. 13). A total of 100 snapshots were taken from this simulation, for which $D = 0.17$. These snapshots were saved every $\Delta t_{snap} = 0.25$, up to time $T = 25$. From these snapshots, the POD modes to be used in the ROM were computed. The first four POD modes for the concentration and temperature are plotted in Fig. 10.

In the first test performed, a POD ROM with five concentration and five temperature modes (so that $2M = 10$) and with $D = 0.17$ is evaluated. The ROM is run until time $T = 100$. Note that this is a much longer time horizon than the time horizon used in the high-fidelity simulation from which the POD basis was generated, and well into the stable limit cycle regime (Fig. 11). The objective here is to test the predictive capability of the ROM for long time simulations. Fig. 11 shows the limit cycles in the

**Note that the current model is a variant of the CDR tubular reactor model developed in [18], but is more efficient, as the BPIM is employed to handle the highly non-linear term appearing in the equation. In [18], the terms involving the projection (85) are treated directly.

Table I. Fluid properties used in the high-fidelity numerical solution of (49)–(52) from which snapshots were taken

Property	Symbol	Value
Péclet number for heat transfer	Pe_H	5.00
Péclet number for mass transfer	Pe_M	5.00
Dimensionless heat of reaction	B	0.50
Dimensionless activation energy	γ	25.0
Dimensionless heat transfer coefficient	β	2.50
Damköhler number	D	0.17
—	θ_0	1

Figure 9. Initial concentration and temperature profiles, y_{in} and θ_{in} for the tubular reactor CDR system

concentration and temperature (the solutions $y(1,t)$ and $\theta(1,t)$ as a function of time) compared with the limit cycles produced by the high-fidelity simulation for two reduced order models: a ROM built using a ten mode (five concentration and five temperature modes) POD basis with a direct treatment of the non-linear terms (plotted in blue), and a ROM built using a ten mode (five concentration and five temperature modes) POD basis with interpolation of the non-linear terms (plotted in red). The boundary conditions in both ROMs are imposed via the penalty formulation outlined in Section 4.1 with $\tau_1 = \tau_2 = 105$. These values are within the stability range derived in Theorem 4.1.1 for a linearization point (y_0, θ_0) with $y_0 \approx -1$ and $\theta_0 > 0.45$, which is in the vicinity of the stable limit cycle. Both reduced order models capture the oscillatory behavior exhibited by the solution (the limit cycle). The red and blue curves in Fig. 11 are indistinguishable, which suggests that the amount of error introduced into the approximation from the interpolation of the non-linear terms is not significant. This observation is confirmed by Fig. 12, which shows the pointwise, time average errors (48) in the concentration y and temperature θ relative to the high-fidelity solution as a function of space with $\tau_1 = \tau_2 = 105$ and $2M = 10$ (five concentration and five temperature) modes. The error is maximal near the right boundary $x = 1$, where a Neumann boundary condition is imposed. Fig. 11 shows that the limit cycle

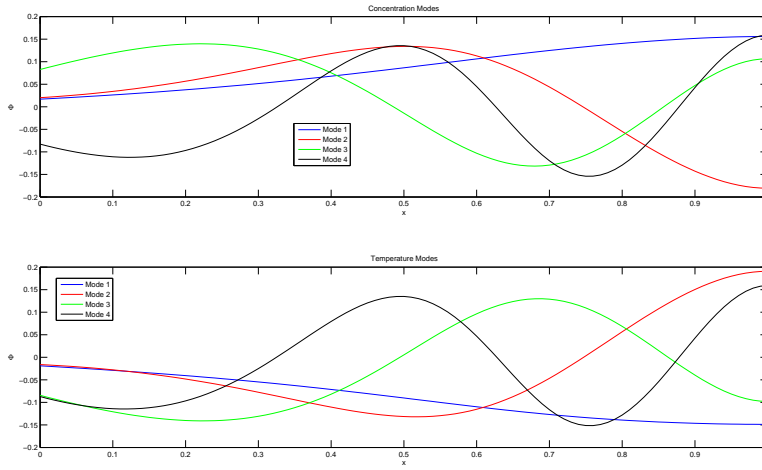


Figure 10. Concentration and temperature POD modes for the tubular reactor CDR system

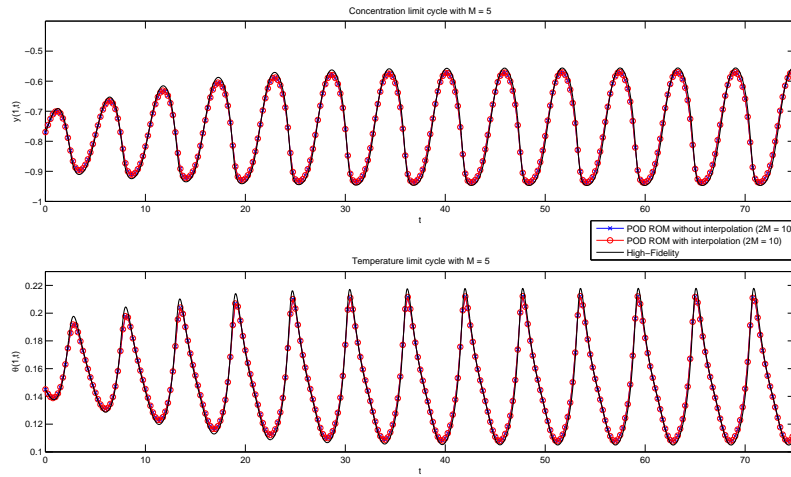


Figure 11. Illustration of limit cycles (y and θ at $x = 1$ as a function of time t) for different ROMs for the tubular reactor CDR system with $2M = 10$ (five concentration and five temperature) modes, $\tau_1 = \tau_2 = 105$ (without and with interpolation)

behavior of the solution is nonetheless captured quite well by the ROMs even at this point of maximal error. The ROM solution with interpolation is slightly less accurate than the ROM solution computed via the direct approach, but only by a very small margin.

In the second test performed, the predictive capability of the ROM with respect to changes in the

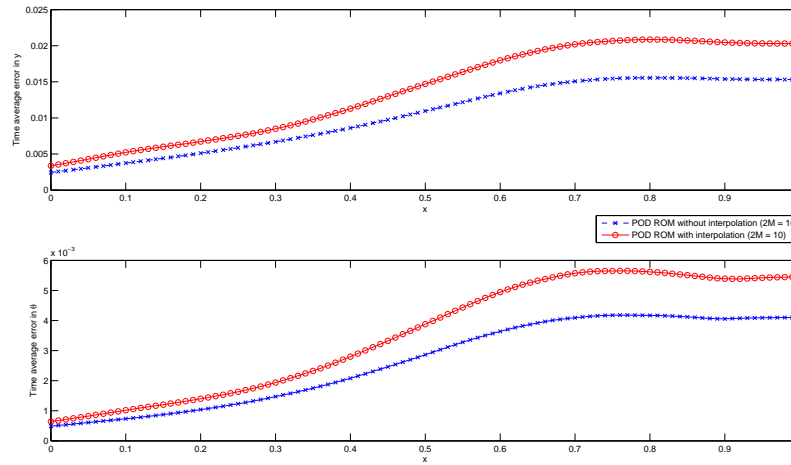


Figure 12. Time-average errors (48) in the ROM solution for the tubular reactor CDR system with $2M = 10$ (five concentration and five temperature) modes, $\tau_1 = \tau_2 = 105$

Damkhöler number is assessed. It is of particular interest whether the ROM can reproduce the bifurcation diagram for this problem. Using the same ten (five concentration and five temperature) mode POD basis described above, computed from snapshots taken up to time $T = 25$ and with $D = 0.17$, solutions to (49) with the boundary conditions (50) and (51) are computed using the ROM for different values of D . Again the ROMs are run for a longer time, until $T = 100$. Fig. 13 compares the bifurcation diagrams obtained for this problem using the high-fidelity model, the ROM without interpolation, and the ROM with interpolation, respectively. The reader can observe that both ROMs predict correctly the existence of stable oscillatory solutions as a function of the Damkhöler number, and identify the lower Hopf bifurcation point $D = 0.165$. The error in the maximum temperature computed by the ROM relative to the maximum temperature computed by the high-fidelity model is in general less than 5% for each value of D . It is interesting to observe that a ROM computed from snapshots taken in an oscillatory regime can still capture well non-oscillatory solutions in the steady regime. Plots of the ROM solutions for $D \neq 0.17$ are not shown here for the sake of brevity.

5. CONCLUSIONS

A technique for building efficient Proper Orthogonal Decomposition (POD)/Galerkin reduced order models (ROMs) for non-linear initial boundary value problems (IBVPs) whose solutions exhibit inherently non-linear behaviors such as metastability and periodic regimes (limit cycles) has been developed. Since the ROM is built by projecting the continuous governing equations onto a set of basis modes, rather than their discretized analogs, enforcement of the boundary conditions by the ROM solution is not automatic. It is observed that the POD modes do not in general satisfy the boundary conditions, particularly if the boundary conditions are of the inhomogeneous, mixed and/or

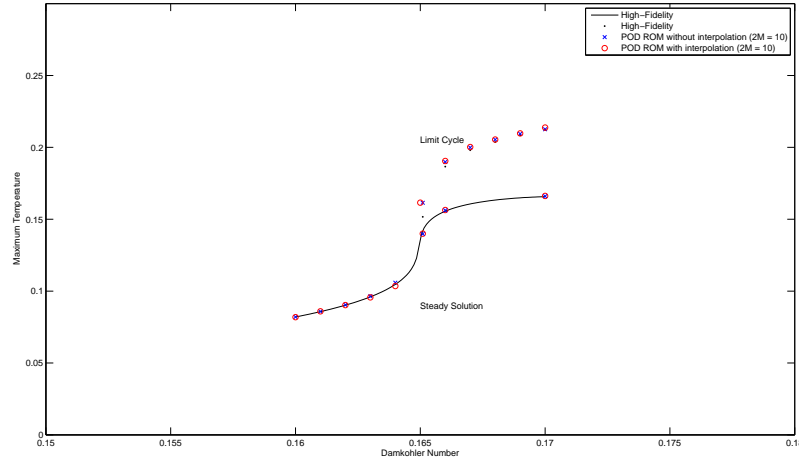


Figure 13. Bifurcation diagram showing the existence of stable oscillatory solutions to the tubular reactor CDR system when $Pe_H = Pe_M = 5$, $B = 0.5$, $\gamma = 25$, $\beta = 2.5$, $\theta_0 = 1$

Robin kind. A formulation in which the boundary conditions are enforced weakly via the penalty method is derived. To determine appropriate values of the penalty parameters, an asymptotic stability analysis of the Galerkin scheme with penalty-enforced boundary conditions is performed, following a linearization and localization of the equations about a stable steady state, similar to the technique employed in [26]. This analysis, borrowed from the spectral method community and performed at the level of the governing (continuous) equations, is made possible by the fact that the *continuous* projection approach is employed in building the ROM. It is emphasized that the same *a priori* stability may not be guaranteed in general for a ROM constructed using the discrete projection approach [14, 4]. As stability is an essential mathematical property of any discretization, including a ROM, and the continuous projection approach can guarantee these results *a priori*, ROMs based on this proposed approach are recommended by the authors despite the additional programming required in implementing such a ROM. Asymptotically stable ROMs with stability-preserving penalty boundary treatment are developed for the Allen-Cahn (or “bistable”) equation as well as a convection-diffusion-reaction (CDR) system representing a tubular reactor. Efficiency of these non-linear reduced order models is maintained by using the “best points” interpolation method (BPIM) to handle the projection of the non-linear terms that are present in these equations. The reduced order models, both without as well as with interpolation, are stable and capture the correct non-linear dynamics of the solutions, namely the phenomenon of metastability for the Allen-Cahn equation and a stable limit cycle for the CDR system.

It is emphasized that the model reduction approach and stability analysis technique proposed herein and illustrated specifically on the two model problems considered can be used to build stable, efficient and accurate ROMs for other non-linear equations in a plethora of applications, following the approach outlined in Section 2.4. The reader is referred to [3] for a discussion of the application of the approach to the compressible Navier-Stokes equations (and other conservation laws), and to [1] for a discussion of a stability-preserving discrete implementation of a ROM constructed using the continuous projection

approach in two and three spatial dimensions.

ACKNOWLEDGEMENTS

This research was funded by Sandia National Laboratories Laboratory Directed Research and Development (LDRD) program. Sandia is a multiprogram laboratory operated by Sandia Corporation, a Lockheed Martin Company for the United States Department of Energy's National Nuclear Security Administration under contract DE-AC04-94AL85000. The first author acknowledges the support of an NDSEG Fellowship sponsored by the U.S. Department of Defense, and also the support of a National Physical Science Consortium (NPSC) Fellowship, funded by the Engineering Sciences Center at Sandia National Laboratories.

REFERENCES

1. M. F. Barone, I. Kalashnikova, D.J. Segalman, H.K. Thornquist. Stable Galerkin Reduced Order Models for Linearized Compressible Flow. *J. Comput. Phys.* **228** (2009) 1932–1946.
2. I. Kalashnikova, M.F. Barone. On the Stability and Convergence of a Galerkin Reduced Order Model (ROM) for Compressible Flow with Solid Wall and Far Field Boundary Treatment. *Int. J. Numer. Meth. Engng.* (2010).
3. I. Kalashnikova, M.F. Barone. Stable and Efficient Galerkin Reduced Order Models for Non-Linear Fluid Flow. *AIAA-2011-3110, 6th AIAA Theoretical Fluid Mechanics Conference*, Honolulu, HI (June 2011).
4. D. Amsallem, C. Farhat. Projection-based Model Reduction with Stability Guarantee. *AIAA-2011-3113, 6th AIAA Theoretical Fluid Mechanics Conference*, Honolulu, HI (June 2011).
5. B. Gustafsson, A. Sundstrom, Incompletely Parabolic Problems in Fluid Dynamics, *SIAM J. Appl. Math.*, **35**(2) (1978) 343–357.
6. J.L. Lumley, Stochastic Tools in Turbulence. New York, NY: Academic Press, 1971.
7. P. Holmes, J.L. Lumley, G. Berkooz, Turbulence, Coherent Structures, Dynamical Systems and Symmetry, New York, NY: Cambridge University Press, 1996.
8. M.F. Barone, J.L. Payne, Methods for Simulation-based Analysis of Fluid-Structure Interaction, *SAND2005-6573*, Sandia National Laboratories, Albuquerque, NM (2005).
9. M. Rathinam, L.R. Petzold, A New Look at Proper Orthogonal Decomposition, *SIAM J. Numer. Anal.* **41** (5) (2003) 1893–1925.
10. K. Kunisch, S. Volkwein, Galerkin Proper Orthogonal Decomposition for a General Equation in Fluid Dynamics, *SIAM J. Numer. Anal.*, **40**(2) (2002) 492–515.
11. L. Sirovich. Turbulence and the dynamics of coherent structures, Part III: Dynamics and scaling. *Quarterly of Appl. Math.* **45** (3) (1987) 583–590.
12. N. Aubry, P. Holmes, J. Lumley, E. Stone. The dynamocs of coherent structures in the wall region of a turbulent boundary layer. *J. Fluid Mech.* **192** (1988) 115–173.
13. K. Veroy, A. T. Patera. Certified real-time solution of the parametrized steady incompressible Navier-Stokes equations: rigorous reduced-bases *a posteriori* error bounds. *Int. J. Num. Meth. Fluids* **47** (2005) 773–788.
14. T. Bui-Thanh, K. Willcox, O. Ghattas, B. van Bloemen Waanders. Goal-oriented, model constrained optimization for reduction of large-scale systems. *J. Comp. Phys.* **224** (2007) 880–896.
15. G. Chen. Stability of Nonlinear Systems. *Encyclopedia of RF and Microwave Engineering*, Wiley, NY, 2004 (pp. 4881–4896).
16. S.M. Allen, J.W. Cahn. A microscopic theory for antiphase boundary motion and its application to antiphase domain coarsening. *Acta Metallurgica* **27** (6) (1979) 1085–1095.
17. R.F. Heinemann, A.B. Poore. Multiplicity, Stability, and Oscillatory Dynamics of the Tubular Reactor. *Chem. Engng. Sci.* **36** (1981) 1411–1419.
18. K. Bizon, G. Continillo, L. Russo, J. Smula. On POD reduced models of tubular reactor with periodic regimes. *Comput. & Chem. Engng.* **32** (2008) 1305–1315.
19. C.W. Rowley, T. Colonius, R.M. Murray. Dynamical Models for Control of Cavity Oscillations. *AIAA Paper* 2001-2126.

20. C.W. Rowley, T. Colonius, R.M. Murray. POD Based Models of Self-sustained Oscillations in the Flow Past an Open Cavity. *AIAA Paper* 2000-1969.
21. O.M. Agudelo, M. Baes, J.J. Espinosa, M. Diehl, B. De Moor. Positive Polynomial Constraints for POD-based Model Predictive Controllers. *IEEE Transactions on Automatic Control* **54** (5) (2009) 988–999.
22. N.C. Nguyen, A.T. Patera, J. Peraire. A ‘best points’ interpolation method for efficient approximation of parametrized functions. *Int. J. Numer. Meth. Engng.* **73**:521–543 (2008).
23. N.C. Nguyen, J. Peraire. An efficient reduced-order modeling approach for non-linear parametrized partial differential equations. *Int. J. Numer. Meth. Engng.* **76**:27–55 (2008).
24. D.J. Bodony, Analysis of Sponge Zones for Computational Fluid Mechanics, *J. Comput. Phys.*, **212** 681-702 (2006).
25. D. Funaro, D. Gottlieb, Convergence results for Pseudospectral Approximations of Hyperbolic Systems by a Penalty-Type Boundary Treatment, *Math. of Comput.* **57**(196) 585-596 (1991).
26. J.S. Hesthaven, D. Gottlieb, A Stable Method for the Compressible Navier-Stokes Equations: I. Open Boundary Conditions, *SIAM J. Sci. Comput.*, **17**(3) 579-612 (1996).
27. L.N. Trefethen. Spectral Methods in MATLAB. SIAM, Philadelphia, 2000.
28. H.O. Kreiss, J. Lorenz. Initial Boundary Value Problems and the Navier-Stokes Equations, *Series in Pure and Applied Mathematics*, Academic Press, San Diego, CA, 1989.
29. E.J. Doedel, R.C. Paffenroth, A.R. Champneys, T.F. Fairgrieve, Y.A. Kuznetsov, B. Sandstede. *et al.* Auto 2000: Continuation and bifurcation software for ordinary differential equations (with HomeCont). Technical report (2001).
30. S. Vazquez, E. Barocia. Analysis of Nonlinear Model Interaction in Stressed Power Systems using POD-Galerkin Characterization. *Int. Conference on Electr. Engng., Comput. Sci. & Auto. Control* (2009) 1–6.
31. S.H. Strogatz. Nonlinear dynamics and chaos: with applications to physics, biology, chemistry, and engineering. Cambridge: Perseus Books, 1994.